

## Article

# Numerical Simulation Study on Gas Migration Patterns in Ultra-Long Fully Mechanized Caving Face and Goaf of High Gas and Extra-Thick Coal Seams

Huaming An <sup>1,2</sup>, Ruyue Gong <sup>1</sup>, Xingxing Liang <sup>1,\*</sup> and Hongsheng Wang <sup>3</sup>

<sup>1</sup> Faculty of Public Security and Emergency Management, Kunming University of Science and Technology, Kunming 650093, China; huaming.an@kust.edu.cn (H.A.); 15612195032@163.com (R.G.)

<sup>2</sup> Geotechnical Institute, TU Bergakademie Freiberg, 09599 Freiberg, Germany

<sup>3</sup> Beijing Chemical Occupational Disease Prevention and Control Institute, Beijing 100093, China; cumming.an@gmail.com

\* Correspondence: xingxingliang@kust.edu.cn

**Abstract:** The purpose of this study is to understand the law of gas migration in the goaf and reduce the gas on the working face. Taking the N2105 working face of the coal mining industry as the research object, the mathematical model of gas seepage in the goaf was established based on the percolation theory of porous media, and the model was solved. Using Fluent software to simulate the initial pressure, the working face airflow, and gas concentration distribution, different ventilation modes of gas concentration distribution and migration law with different wind speeds after the initial gas pressure. It is concluded that for the first time, the effect of gas on the working face is insignificant, and the influence of the initial pressure on the working surface is gradually revealed. The influence of airflow speed on the goaf is mainly concentrated in the 20~30 m area near the working face, which is affected by the airflow speed of the working face. The gas concentration in the goaf is low, and the fluctuation is obvious. The types of ventilation directly affect the seepage law of goaf gas. The U + I and U + L type ventilation can reduce the gas concentration in the upper corner and f gas seepages from goaf to the working face.



Academic Editors: Hengrui Liu and Anthony Chun Yin Yuen

Received: 6 November 2024

Revised: 18 December 2024

Accepted: 24 December 2024

Published: 31 December 2024

**Citation:** An, H.; Gong, R.; Liang, X.; Wang, H. Numerical Simulation Study on Gas Migration Patterns in Ultra-Long Fully Mechanized Caving Face and Goaf of High Gas and Extra-Thick Coal Seams. *Fire* **2025**, *8*, 13. <https://doi.org/10.3390/fire8010013>

**Copyright:** © 2024 by the authors. Licensee MDPI, Basel, Switzerland. This article is an open access article distributed under the terms and conditions of the Creative Commons Attribution (CC BY) license (<https://creativecommons.org/licenses/by/4.0/>).

**Keywords:** goaf areas; component transport; gas accumulation; numerical simulation

## 1. Introduction

Fully mechanized top coal caving mining is a new mining technology with high yield and high efficiency. However, due to its large mining intensity, fast propulsion speed, short gas pre-discharge time of the coal wall, large gas emission from the working face (coal body of the working face, caving coal body, coal wall including coal wall above support, and residual coal in goaf, etc.), it is easy to cause gas accumulation or gas overrun in the mining area, upper corner, and mine return airway. Gas overrun has caused serious threats, hazards, and hidden dangers to coal mine safety production, which may cause safety accidents such as gas explosion and gas suffocation, causing great property losses and casualties to the country, enterprises, and individuals [1–4].

Aiming at the problem of gas hidden danger in the working face and goaf of high gas and extra-thick coal seams, in recent years, scholars have extensively discussed the theoretical analysis, numerical simulation, and experimental research on gas migration in the working face and goaf and put forward and promoted gas control measures such as pre-drainage before mining, simultaneous excavation and drainage, simultaneous mining and

drainage, high-drainage drilling, buried pipe drainage in upper corners, and increasing air distribution and gas drainage in high-level roadways along the roof layout of the working face. A series of useful research results have been formed. For example, in 2007, taking the Riosa-Olloniego coalfield coal mine in Spain as the engineering background, Aguado and Nicieza compared and analyzed the effectiveness of two important measures to prevent coal seam gas outburst, e.g., high-pressure water injection and protective coal seam (No. 7 coal seam) [5]. In 2011, Zhu Zhengong, Guo Liangjing, Wang Xiang, and others used experimental methods to optimize the ventilation system of a fully mechanized caving face, reducing the accumulation of gas [6]. In 2013, Zhao Jinqiang studied the gas emission law of a fully mechanized top coal caving face and analyzed its influencing factors [7]. In 2014, Hao Yabing et al. studied the effect of parallel double U-shaped ventilation on gas accumulation [8]. In 2015, in order to prevent the formation gas from entering and submerging the mine ventilation system, Karacan put forward the control measures of drilling the goaf gas vents (GGVs) on the long wall plate to reduce the gas content and deeply analyzed the production performance of GGVs [9]. In 2016, Li Yanqing discussed the gas control method of the outburst coal seam group [10]. In 2018, Zhang Xuechao and Chang Weiqi explored and practiced gas control work such as high gas coal seam groups and fully mechanized caving faces [11,12]. Zhou et al. studied the extraction effect of high-level drainage roadway in fully mechanized mining face [13]. In 2022, Shi Liangliang studied the gas control technology in the goaf of the fully mechanized mining face [14]. Huang Maozheng studied the relationship between coal seam gas occurrence conditions and flow theory [15]. Lin Haifei et al. used experimental methods to study the influence of multiple factors on the gas adsorption of coal samples [16]. Xin Yulun and Zhou Yanyang et al. carried out systematic research on gas in layered mining of high gas thick coal seams [17,18] and so on and achieved remarkable results in gas drainage and gas control in the working face. Additionally, in 2023, Karacan proposed a comprehensive alternative to the coal seam mining scheme of the Pocahontas No. 3 coal bed in Virginia (Central Appalachian Basin), USA, including the comprehensive application of different methods (e.g., fracturing vertical wells, horizontal wells in coal seams, and gas vents (GGVs) in goafs), as well as the determination of the optimal duration and arrangement of different prevention and control measures [19].

However, the production practice also exposed that the unreasonable gas layout of the pre-drainage coal seam and the mismatch of ventilation parameter settings lead to gas accumulation in the working face, upper corner, and goaf, and even the gas concentration exceeds the limit. Due to the non-reproducibility of the mining process, gas hazards often occur. As a simple, economical, practical, and repeatable research method, numerical simulation has been widely used in gas migration and control. Soleimani et al. used the energy balance principle to numerically model the initiation of coal and natural gas outbursts, successfully simulated the gas outburst caused by deformed coal, and focused on predicting the initiation of gas outbursts by using thresholds [20]. Szott et al. proposed the technology of promoting gas seepage and emission by stimulating coal seams in a multi-coal seam mining layout through a numerical simulation method [21]. Hu Qianting used the CFD simulation of the gas flow law in the goaf to study the gas migration law in the goaf [22]. Li Zongxiang conducted a numerical simulation study on the gas emission law in the goaf of the fully mechanized caving face [23]. Zhang Yunzeng studied the gas concentration distribution and migration law in the goaf of the fully mechanized mining face through experimental methods [24]. Yu Yanan et al. conducted a numerical simulation study on the air leakage field and gas flow field in the goaf of the “Y” type ventilation system [25,26], which provided a basis for the improvement of coal mine technology.

However, these studies are highly targeted, and there is a lack of simulation analysis of the comprehensive factors affecting gas accumulation in mining, such as coal body in working face, caving coal body, coal wall, and residual coal in goaf. How to theoretically demonstrate and discuss the problem of gas concentration exceeding the limit caused by gas accumulation caused by various comprehensive factors and find laws and methods to fundamentally solve the problem of gas exceeding the limit in the working face and upper corner of fully mechanized caving mining in high gas and extra-thick coal seams.

In order to effectively deal with the problem of gas accumulation and overrun in fully mechanized caving mining of high gas and ultra-thick coal seams, this paper takes the N2105 working face of a coal mine as the prototype and uses the method of numerical simulation to deeply discuss the influencing factors of gas accumulation in the working face, upper corner, and goaf. The influence degree and law of gas accumulation caused by different factors, such as airflow speed of the working face, advancing speed of the working face, ventilation mode of the working face, residual coal in goaf, and residual gas in coal seam, are studied and analyzed, which provides technical support for the selection of gas control process parameters in fully mechanized caving mining.

## 2. Study on Gas Migration Law in Fully Mechanized Caving Face and Goaf

The study of gas migration law in fully mechanized caving face and goaf focuses on the non-chemical reaction single-phase multi-component diffusion model of gas moving with airflow in confined space and the establishment of a mathematical model of gas seepage in goaf and its equation solution.

### 2.1. Establishment and Solution of Mathematical Model of Gas Diffusion in Fully Mechanized Caving Face

#### 2.1.1. Establishment of Mathematical Model of Gas Diffusion in Fully Mechanized Caving Face

The movement of gas with airflow in a confined space is a single-phase, multi-component diffusion problem without chemical reaction. Its motion law satisfies the basic equations of fluid mechanics described by the general Navier–Stokes equations, including the continuity equation, momentum conservation equation, energy conservation equation, component mass conservation equation, turbulent kinetic energy ( $k$ ) equation, and turbulent frequency equation ( $\omega$ ) for turbulent airflow in confined space [27–30].

The mathematical expression of the Navier–Stokes equation has two different basic forms: differential form and integral form. Suppose the volume force and external heat source are not considered. In that case, in the rectangular coordinate system, the conservative integral form of the three-dimensional N–S equations of incompressible flow is:

$$\frac{\partial}{\partial t} \iiint_{\Omega} Q d\Omega + \iint_{\partial\Omega} F_c \cdot nds = \iint_{\partial\Omega} F_v \cdot nds \tag{1}$$

among them,

$$Q = \begin{bmatrix} \rho \\ \rho u \\ \rho v \\ \rho w \\ \rho E \end{bmatrix} \quad F_v = \begin{bmatrix} 0 & 0 & 0 \\ \tau_{xx} & \tau_{yx} & \tau_{zx} \\ \tau_{xy} & \tau_{yy} & \tau_{zy} \\ \tau_{xz} & \tau_{yz} & \tau_{zz} \\ \varphi_x & \varphi_y & \varphi_z \end{bmatrix} \tag{2}$$

$$\varphi_x = u\tau_{xx} + v\tau_{xy} + w\tau_{xz} + q_x \tag{3}$$

$$\varphi_y = u\tau_{yx} + v\tau_{yy} + w\tau_{yz} + q_y \tag{4}$$

$$\varphi_z = u\tau_{zx} + v\tau_{zy} + w\tau_{zz} + q_z \tag{5}$$

$$\tau_{xx} = -\frac{2}{3}\mu(u_x + v_y + w_z) + 2\mu u_x \tag{6}$$

$$\tau_{yy} = -\frac{2}{3}\mu(u_x + v_y + w_z) + 2\mu u_y \tag{7}$$

$$\tau_{zz} = -\frac{2}{3}\mu(u_x + v_y + w_z) + 2\mu u_z \tag{8}$$

$$\tau_{xy} = \tau_{yx} = \mu(u_y + v_x) \tag{9}$$

$$\tau_{xz} = \tau_{zx} = \mu(u_z + w_x) \tag{10}$$

$$\tau_{yz} = \tau_{zy} = \mu(v_z + w_y) \tag{11}$$

where  $\partial\Omega$  represents the boundary of the control volume,  $N$  is the outer normal vector of the boundary,  $Q$  is the conserved variable,  $F_c$  is the inviscid flux, and  $F_v$  is the viscous flux.  $\tau_{xx}$ ,  $\tau_{yy}$ , and  $\tau_{zz}$  represents the viscous stress component in different directions,  $q_x$ ,  $q_y$ , and  $q_z$  and represents the heat flux in different directions.  $\rho$ ,  $P$ , and  $E$  represent the total energy of density, static pressure, and unit mass, respectively, and  $u$ ,  $a$ ,  $w$  represent the velocity component in the direction of  $x$ ,  $y$ ,  $z$  in the Cartesian coordinate system.

In order to close the N–S equation, some relational expressions need to be supplemented. For single-phase gas, there is a state equation:

$$p = \rho RT \tag{12}$$

Unit mass gas total energy equation:

$$E = e + \frac{1}{2}(u^2 + v^2 + w^2) \tag{13}$$

Based on the eddy viscosity hypothesis, the viscosity coefficient  $\mu = \mu_I + \mu_T$ , where  $\mu_I$  is the laminar viscosity coefficient, given by the Sutherland formula,  $\mu_T$  is the turbulent viscosity coefficient, given by the turbulence model.

The laminar viscosity coefficient  $\mu_I$  can be expressed as:

$$\mu_I = T^{\frac{3}{2}} \cdot \frac{1 - S}{T + S} \tag{14}$$

$$S = \frac{124K}{T_\infty} \tag{15}$$

The turbulent viscosity coefficient  $\mu_T$  formula is:

$$\mu_T = \frac{\rho k}{\omega} \tag{16}$$

The turbulent viscosity coefficient  $\mu_T$  is determined by solving the turbulent kinetic energy ( $k$ ) equation and the turbulent frequency ( $\omega$ ) equation.

The  $k$  equation and the  $\omega$  equation are:

$$\frac{\partial(\rho k)}{\partial t} + \frac{\partial}{\partial x_j} \left[ \rho u_j k - (\mu + \sigma_k \mu_T) \frac{\partial k}{\partial x_j} \right] = \tau_{tij} S_{ij} - \beta' \rho k \omega \tag{17}$$

$$\frac{\partial(\rho \omega)}{\partial t} + \frac{\partial}{\partial x_j} \left[ \rho u_j \omega - (\mu + \sigma_\omega \mu_T) \frac{\partial \omega}{\partial x_j} \right] = \alpha \frac{\omega}{k} \tau_{tij} S_{ij} - \beta \rho \omega^2 \tag{18}$$

among them,

$$\tau_{tij} = 2\mu_T \left( S_{ij} - \frac{S_{mn} \delta_{ij}}{3} \right) - \frac{2}{3} \rho k \delta_{ij} \tag{19}$$

where  $S_{ij}$  is the average velocity strain tensor,  $\rho$  represents the fluid density,  $k$  represents the turbulent kinetic energy,  $\delta_{ij}$  is the Kronecker operator, and  $\tau_{ij}$  is the Reynolds stress.  $\alpha = \frac{5}{9}$ ,  $\beta' = 0.09$ ,  $\beta = 0.075$ ,  $\sigma_k = 0.5$  and  $\sigma_\omega = 0.5$ .

At this point, the establishment of the mathematical model of the whole problem is completed.

### 2.1.2. Solution of Gas Diffusion Equation in Working Face

In this paper, the finite volume method with a spatial discretization scheme is used to solve the N–S equation describing gas diffusion, and the equation is discretized into algebraic equations with the physical quantity at the center of the grid unit as the unknown quantity [31,32].

On any control unit  $\Omega_{ijk}$  in the working face space, the N–S equation in the integral form can be expressed as:

$$\frac{\partial}{\partial t} \iiint_{\Omega_{i,j,k}} Q d\Omega + \iint_{\partial\Omega_{i,j,k}} F_c \cdot n ds = \iint_{\partial\Omega_{i,j,k}} F_v \cdot n ds \tag{20}$$

The control volume boundary  $\partial\Omega_{i,j,k}$  is composed of six surfaces of the control unit, namely:

$$\partial\Omega_{i,j,k} = ds_{i-\frac{1}{2},j,k} + ds_{i+\frac{1}{2},j,k} + ds_{i,j-\frac{1}{2},k} + ds_{i,j+\frac{1}{2},k} + ds_{i,j,k-\frac{1}{2}} + ds_{i,j,k+\frac{1}{2}} \tag{21}$$

The flow  $Q_{i,j,k}$  is the volume average of the cell center, namely:

$$Q_{i,j,k} = \frac{1}{V_{i,j,k}} \iiint_{\Omega_{i,j,k}} Q d\Omega \tag{22}$$

the element volume  $V_{i,j,k}$  can be calculated by the surface vector  $s_{i-\frac{1}{2},j,k}$ ,  $s_{i,j-\frac{1}{2},k}$ ,  $s_{i,j,k-\frac{1}{2}}$  and its main diagonal vector  $r_{i,j,k}$ .

$$r_{i,j,k} = (x_{i+1,j+1,k+1} - x_{i,j,k})l_x + (y_{i+1,j+1,k+1} - y_{i,j,k})l_y + (z_{i+1,j+1,k+1} - z_{i,j,k})l_z \tag{23}$$

$$V_{i,j,k} = \frac{1}{3} r_{i,j,k} \cdot (ds_{i-\frac{1}{2},j,k} + ds_{i,j-\frac{1}{2},k} + ds_{i,j,k-\frac{1}{2}}) \tag{24}$$

where  $ds$  is the area vector of the element, and  $ds_{i-\frac{1}{2},j,k}$  is calculated by the following formula:

$$ds_{i-\frac{1}{2},j,k} = \frac{1}{2} (a_{i-\frac{1}{2},j,k} \times b_{i-\frac{1}{2},j,k}) \tag{25}$$

where  $a$  and  $b$  are the two diagonal vectors of the directed surface  $ds$ , which are expressed as:

$$a_{i-\frac{1}{2},j,k} = (x_{i,j+1,k+1} - x_{i,j,k})l_x + (y_{i,j+1,k+1} - y_{i,j,k})l_y + (z_{i,j+1,k+1} - z_{i,j,k})l_z \tag{26}$$

$$b_{i-\frac{1}{2},j,k} = (x_{i,j,k+1} - x_{i,j+1,k})l_x + (y_{i,j,k+1} - y_{i,j+1,k})l_y + (z_{i,j,k+1} - z_{i,j+1,k})l_z \tag{27}$$

where  $l_x$ ,  $l_y$ ,  $l_z$  are unit vectors along the rectangular coordinates  $x$ ,  $y$ ,  $z$ .

Equation (22) is discretized into the following form:

$$\frac{d}{dt} (V_{i,j,k} Q_{i,j,k}) + W_{c,i,j,k} - W_{v,i,j,k} = 0 \tag{28}$$

where  $W_c$  and  $W_v$  are the net flow rate and net viscous flux of the outflow grid unit, respectively.

$$\begin{aligned}
 W_{c,i,j,k} &= \sum F_c \cdot ds \\
 &= F_{c_{i+\frac{1}{2},j,k}} \cdot ds_{i+\frac{1}{2},j,k} - F_{c_{i-\frac{1}{2},j,k}} \cdot ds_{i-\frac{1}{2},j,k} + F_{c_{i,j+\frac{1}{2},k}} \cdot ds_{i,j+\frac{1}{2},k} - F_{c_{i,j-\frac{1}{2},k}} \cdot ds_{i,j-\frac{1}{2},k} + F_{c_{i,j,k+\frac{1}{2}}} \cdot ds_{i,j,k+\frac{1}{2}} \\
 &\quad - F_{c_{i,j,k-\frac{1}{2}}} \cdot ds_{i,j,k-\frac{1}{2}}
 \end{aligned} \tag{29}$$

where  $ds$  is the directed area of the unit interface, and the convective flux on the unit interface is taken as the average value on the adjacent two units, that is:

$$F_{c_{i\pm\frac{1}{2},j,k}} = \frac{1}{2} (F_{c_{i,j,k}} + F_{c_{i\pm 1,j,k}}) \tag{30}$$

$$F_{c_{i,j\pm\frac{1}{2},k}} = \frac{1}{2} (F_{c_{i,j,k}} + F_{c_{i,j\pm 1,k}}) \tag{31}$$

$$F_{c_{i,j,k\pm\frac{1}{2}}} = \frac{1}{2} (F_{c_{i,j,k}} + F_{c_{i,j,k\pm 1}}) \tag{32}$$

For the viscous flux, the thin layer approximation can be expressed as:

$$W_v = W_{v\zeta} + W_{v\eta} + W_{v\zeta} \tag{33}$$

Taking the  $\zeta$  direction as an example, the expression of the viscous flux is given. The viscous flux in the  $\eta$  and  $\zeta$  directions have a similar expression with the viscous flux in the direction.

$$W_{v\zeta} = \begin{bmatrix} 0 \\ \varphi_1 u_\zeta + S_{\zeta x} \varphi_2 \\ \varphi_1 v_\zeta + S_{\zeta y} \varphi_2 \\ \varphi_1 w_\zeta + S_{\zeta z} \varphi_2 \\ \varphi_1 [(q^2/2) \cdot \zeta + 1/((r-1)Pr)] + \bar{U} \varphi_2 \end{bmatrix} \tag{34}$$

$$\varphi_1 = S_{\zeta x}^2 + S_{\zeta y}^2 + S_{\zeta z}^2 \tag{35}$$

$$\varphi_2 = \frac{1}{3} (S_{\zeta x} u_\zeta + S_{\zeta y} v_\zeta + S_{\zeta z} w_\zeta) \tag{36}$$

$$q^2 = u^2 + v^2 + w^2 \tag{37}$$

$$\bar{U} = S_{\zeta x} u + S_{\zeta y} v + S_{\zeta z} w \tag{38}$$

where  $S_{\zeta x}$ ,  $S_{\zeta y}$ ,  $S_{\zeta z}$  are the components of the directed area of the unit interface in the  $\zeta$  direction.

So far, the FCD model has been used to solve the gas flow equation of the working face.

## 2.2. Establishment and Solution of Mathematical Model of Gas Seepage in Goaf

### 2.2.1. Establishment of Mathematical Model of Gas Seepage in Goaf

In the process of establishing the mathematical model of gas migration law in the goaf of the working face, the desorption and diffusion process of the residual coal gas is ignored, and only the seepage process in the porous medium formed by the caving coal and rock mass in the goaf of the working face is considered. The gas flow in the goaf follows the mass conservation equation, momentum conservation equation, and continuity equation. Without considering gravity, due to the continuous gas in the surrounding rock and residual coal in the goaf, the transport of gas in the goaf should be regarded as a

continuous source distribution in the continuity equation. Hence, the transport of gas in the goaf satisfies the law of conservation of gas mass [33–36].

$$\frac{\partial}{\partial t}(\rho c_g) + \frac{\partial}{\partial x_i}(\rho c_g \bar{u}) = -\frac{\partial}{\partial x_i}(J_g \bar{u}) + S_g \quad (39)$$

The diffusion flux of gas in laminar flow is:

$$J_g = -D\rho \frac{\partial}{\partial x_i}(c_g u_i) \quad (40)$$

The diffusion flux of gas in turbulent flow is:

$$J_g = -\left(D\rho + \frac{\mu_t}{Sc_t}\right) \frac{\partial}{\partial x_i}(c_g u_i) \quad (41)$$

The average gas velocity is regarded as the macroscopic seepage velocity, namely:

$$\bar{u} = -\frac{K}{\mu} \nabla p \quad (42)$$

Substituting Equations (40) and (41) and Equations (40) and (42) into Equation (39), respectively, the continuous equations expressed by seepage velocity in laminar and turbulent flows can be obtained:

The continuous equation expressed by seepage velocity in laminar flow:

$$\frac{\partial}{\partial t}(\rho c_g) + \frac{\partial}{\partial x_i}(-\rho c_g \frac{K_g}{\mu_g} \nabla P_g) = -\frac{\partial}{\partial x_i} \left[ D\rho \frac{\partial}{\partial x_i}(c_g u_i) \frac{K_g}{\mu_g} \nabla P_g \right] + S_g \quad (43)$$

The continuous equation expressed by seepage velocity in turbulent flow:

$$\frac{\partial}{\partial t}(\rho c_g) + \frac{\partial}{\partial x_i}(-\rho c_g \frac{K_g}{\mu_g} \nabla P_g) = -\frac{\partial}{\partial x_i} \left\{ \left[ \left( D\rho + \frac{\mu_t}{Sc_t} \right) \frac{\partial}{\partial x_i}(c_g u_i) \right] \frac{K_g}{\mu_g} \nabla P_g \right\} + S_g \quad (44)$$

The gas migration in the caving coal and rock mass in the goaf satisfies the law of conservation of momentum, and the momentum conservation equation in the  $i$  direction in the inertial (non-accelerating) coordinate system is:

$$\frac{\partial}{\partial t}(\rho u_i) + \frac{\partial}{\partial x_j}(\rho u_i u_j) = \frac{\partial \tau_{ij}}{\partial x_j} - \frac{\partial p}{\partial x_i} + \rho g_i + F_i \quad (45)$$

$$\tau_{ij} = \left[ u_{eff} \left( \frac{\partial u_i}{\partial x_j} + \frac{\partial u_j}{\partial x_i} \right) - \frac{2}{3} \frac{\partial u_i}{\partial x_j} \delta_{ij} \right] \quad (46)$$

Substituting (46) into (45) yields:

$$\frac{\partial}{\partial t}(\rho u_i) + \frac{\partial}{\partial x_j}(\rho u_i u_j) = \frac{\partial}{\partial x_j} \left( u_{eff} \frac{\partial u_i}{\partial x_j} \right) + \frac{\partial}{\partial x_j} \left( u_{eff} \frac{\partial u_j}{\partial x_i} \right) - \frac{2}{3} \frac{\partial}{\partial x_j} \left( \frac{\partial u_j}{\partial x_j} \right) - \frac{\partial p}{\partial x_i} + \rho g_i + F_i \quad (47)$$

when,

$$Q_i = \frac{\partial}{\partial x_j} \left( u_{eff} \frac{\partial u_j}{\partial x_i} \right) - \frac{2}{3} \frac{\partial}{\partial x_i} \left( \frac{\partial u_j}{\partial x_j} \right) + F_i \quad (48)$$

When the momentum conservation equations in the x, y, z directions in the inertial (non-accelerating) coordinate system are:

$$\frac{\partial}{\partial t}(\rho u_x) + \frac{\partial}{\partial x_j}(\rho u_x u_j) = \frac{\partial}{\partial x_j} \left( u_{eff} \frac{\partial u_x}{\partial x_j} \right) - \frac{\partial p}{\partial x} + \rho g_x + Q_x \quad (49)$$

$$\frac{\partial}{\partial t}(\rho u_y) + \frac{\partial}{\partial x_j}(\rho u_y u_j) = \frac{\partial}{\partial x_j} \left( u_{eff} \frac{\partial u_y}{\partial x_j} \right) - \frac{\partial p}{\partial y} + \rho g_y + Q_y \quad (50)$$

$$\frac{\partial}{\partial t}(\rho u_z) + \frac{\partial}{\partial x_j}(\rho u_z u_j) = \frac{\partial}{\partial x_j} \left( u_{eff} \frac{\partial u_z}{\partial x_j} \right) - \frac{\partial p}{\partial z} + \rho g_z + Q_z \quad (51)$$

The source term of porous media consists of two parts: one is the viscous loss term, and the other is the internal loss term, namely:

$$F_i = \sum_{j=1}^3 D_{ij} u_{eff} q_j + \sum_{j=1}^3 C_{ij} \frac{1}{2} \rho |q_j| q_j \quad (52)$$

### 2.2.2. Solution of Gas Seepage Equation in Goaf

The model is selected to solve the gas flow equation in the goaf. The model is derived from the transient Navier–Stokes equation by Yanhot and Orzag using the renormalization group method. It is mainly composed of the turbulent kinetic energy (*k*) equation and the turbulent kinetic energy dissipation rate ( $\epsilon$ ) diffusion equation, which is completed by the tensor notation under the Einstein summation convention [31,37–40].

$$\frac{\partial}{\partial t}(\rho k) + \frac{\partial}{\partial_i}(\rho k u_i) = \frac{\partial}{\partial x_j} \left( \alpha_k \mu_{eff} \frac{\partial k}{\partial x_j} \right) + G_k + G_b - \rho \epsilon - Y_M \quad (53)$$

$$\frac{\partial}{\partial t}(\rho \epsilon) + \frac{\partial}{\partial_i}(\rho \epsilon u_i) = \frac{\partial}{\partial x_j} \left( \alpha_\epsilon \mu_{eff} \frac{\partial \epsilon}{\partial x_j} \right) + C_{1\epsilon} \frac{\epsilon}{k} (G_k + C_{3\epsilon} G_b) - C_{2\epsilon} \rho \frac{\epsilon^2}{k} - R_\epsilon + S_\epsilon \quad (54)$$

where

$$G_k = \mu_t \left( \frac{\partial u_i}{\partial x_j} + \frac{\partial u_j}{\partial x_i} \right) \frac{\partial u_i}{\partial x_j} \quad (55)$$

$$G_b = -g_i \frac{\mu_t}{\rho Pr_t} \frac{\partial \rho}{\partial x_i} \quad (56)$$

$$R_\epsilon = \frac{C_\mu \rho \eta (1 - \eta / \eta_0)}{1 + \beta \eta^3} \cdot \frac{\epsilon^2}{k} \quad (57)$$

$$\eta = (2E_{ij} \cdot E_{ij})^{1/2} \frac{k}{\epsilon} \quad (58)$$

$$E_{ij} = \frac{1}{2} \left( \frac{\partial u_i}{\partial x_j} + \frac{\partial u_j}{\partial x_i} \right) \quad (59)$$

At the same time, in the RNG model, in order to make the model adapt to the influence of near-wall flow, low Reynolds number, and modified turbulence in laminar flow by eddy current, it is necessary to include the effective velocity and eddy current modified model equation, that is:

$$d \left( \frac{\rho^2 k}{\sqrt{\mu \epsilon}} \right) = 1.72 \frac{\hat{v}}{\sqrt{\hat{v}^3 - 1 + C_v}} d \hat{v} \quad (60)$$

For turbulence there is:

$$\mu_t = C_\mu \rho \frac{k^2}{\varepsilon} \quad (61)$$

For eddy currents there is:

$$\mu_t = \eta_{t0} f(\alpha_s, \Omega, k/\varepsilon) \quad (62)$$

where  $S_g$  is the additional generation rate of the gas source term,  $c_g$  is the gas concentration in the goaf,  $\phi$  is the porosity of the collapsed coal and rock mass in the goaf,  $J_g$  is the gas diffusion flux,  $\bar{u}$  is the average seepage velocity of the gas in the goaf,  $D$  is the diffusion coefficient of the gas in the mixed gas,  $Sc_t$  is the turbulent Schmidt number, generally 0.7,  $u_i$  is the gas seepage velocity in the goaf,  $P$  is the pressure,  $K$  is the permeability of the goaf,  $\mu$  is the gas viscosity,  $\tau_{ij}$  is the stress tensor,  $u_i$  is the time average velocity,  $\alpha_k$  and  $\alpha_\varepsilon$  are the turbulent Prandtl number of the equation  $k$  and the equation  $\varepsilon$ , and  $G_b$  is the turbulent kinetic energy caused by buoyancy.

The RNG  $k - \varepsilon$  model is used to solve the gas flow equation in the goaf, which satisfies the stability and economic requirements of the solution process and makes the accuracy higher when calculating the flow field with a large gradient of calculation speed; that is, the solution of the gas flow equation under the condition of high Reynolds number is realized, and the solution of the equation under the condition of low Reynolds number in the near wall area is realized.

In this section, we deeply discussed the law of gas migration in a fully mechanized caving face and goaf, established a mathematical model of multi-component diffusion without chemical reaction, and based on porous media seepage, and solved the mathematical model. This study not only provides a theoretical basis for the transport characteristics of gas in the working face and goaf but also reveals the influence of the continuous release of residual coal and surrounding rock gas on the concentration distribution in the working face and goaf. The establishment and solution of the model are of great significance for understanding the gas seepage mechanism, optimizing the safety of mining operations, and reducing the risk of gas disasters, which lays a solid foundation for future related research and practical application.

### 3. Establishment of Geometric Model and the Determination of Simulation Parameters

This section introduces the establishment process of the geometric model of the working face and the goaf. According to the theory of surrounding rock mass deformation and the needs of numerical simulation, a three-dimensional geometric model including the working face, the air inlet roadway, the return air roadway, and the gas roadway is constructed, and the simulated boundary conditions are set.

#### 3.1. Establishment of Geometric Model of Working Face and Goaf and the Setting of Boundary Conditions

The coal seam thickness of the N2105 working face in the coal mine of Shanxi Province, China is 6.31 m, the mining height of the working face is  $3.2 \pm 0.1$  m, the average thickness of top coal is 3.11 m, and the inclined distance of the cutting hole in the working face is 285 m. The schematic figure of the section of the fully mechanized caving face is shown in Figure 1.

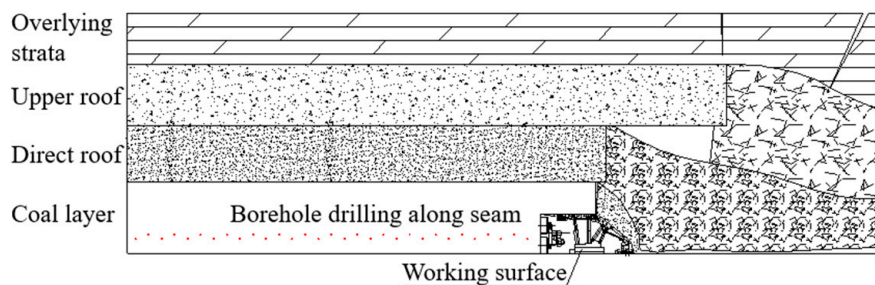


**Figure 1.** The schematic figure of fully mechanized caving face and goaf areas.

According to the actual situation, the model of the fully mechanized caving face is simplified. The rocker arm and fuselage of the shearer are simplified as cuboids, drums and hydraulic supports are simplified as cylinders, and cable grooves are simplified as cuboids. A trapezoidal working face with a length of 285 m, a width of 8.5 m, and a height of 3.5 m is established. The length, width, and height of inlet and return air lanes are 15 m, 5 m, and 3.5 m, respectively. The length, width, and height of gas lanes are 20 m, 4.4 m, and 3.5 m, respectively. The working face and goaf geometric model with a strike length of 200 m, a tendency length of 285 m (including inlet and return air lanes), and a vertical height of 40 m are shown in Figure 2.

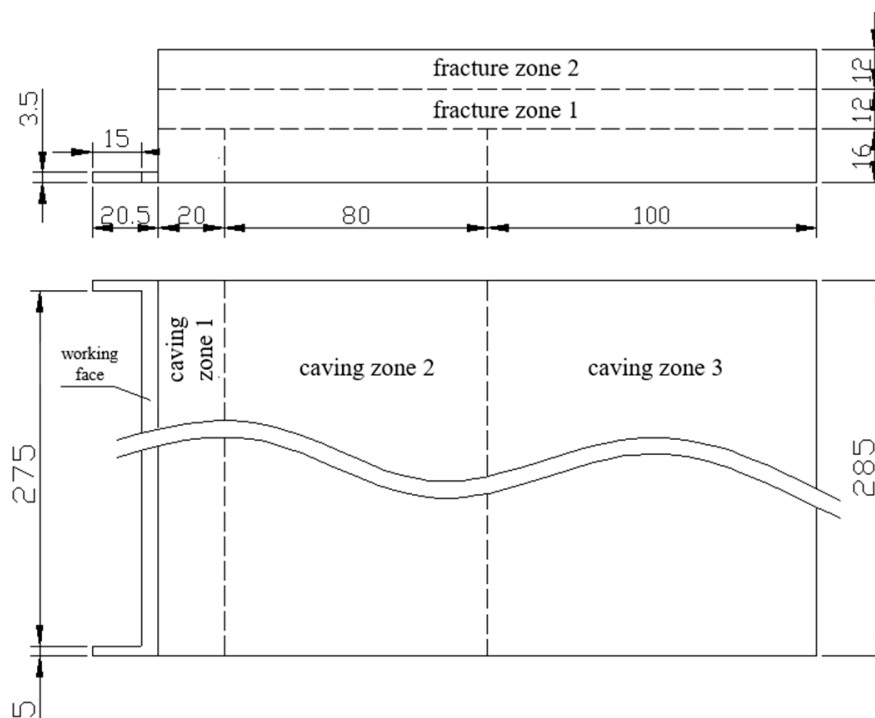


**Figure 2.** Fully mechanized caving face and goaf geometry size figure.

### 3.2. Setting of Boundary Conditions of Working Face and Goaf Areas

According to the actual parameters and measured data of the N2105 working face and the adaptive adjustment of the comprehensive regional grid, the numerical simulation parameters of gas migration law in the fully mechanized caving face are set in Table 1, and the numerical simulation parameters of gas migration law in goaf are set in Table 2.

**Table 1.** Working face gas diffusion numerical simulation parameter setting table.

Simulated Boundary Condition	Simulation Parameter Setting
Equation solver	Separation solver
Turbulent flow model	$\kappa$ - $\epsilon$ two-equation model
Component model	Gas-air
Energy model	Open
Convergence criteria	$10^{-3}$
Porous media model	Open
Percentage of void	0.2
Inertial resistance coefficient ( $1/m^2$ )	$1.0 \times 10^5$
Type of jet source	Body spray
Material quality	Methane
Density ( $kg/m^3$ )	0.716
Total mass flow rate of injection source	$1.5 \times 10^{-7}$

**Table 2.** Simulation parameters of gas migration law in goaf areas.

Name	Fall Zone 1	Fall Zone 1	Fall Zone 1	Fissure Zone 1	Fissure Zone 1
Porosity	0.333	0.231	0.167	0.05	0.02
Coefficient of viscous Resistance ( $10^7 m^{-2}$ )	0.7	1.5	5	100	200
Methane source term	0.043	0.147	0.17	0.25	0.06

#### 4. Numerical Simulation of Gas Migration Law in Working Face and Goaf

##### 4.1. Simulation Study on the Distribution Law of Air Flow Field in Fully Mechanized Caving Face

Taking the airflow speed of 2.92 m/s as an example, the distribution law of the airflow field in the working face is simulated. The distribution cloud figure of the airflow field in a fully mechanized caving face is shown in Figure 3, and the vector figure is shown in Figure 4.

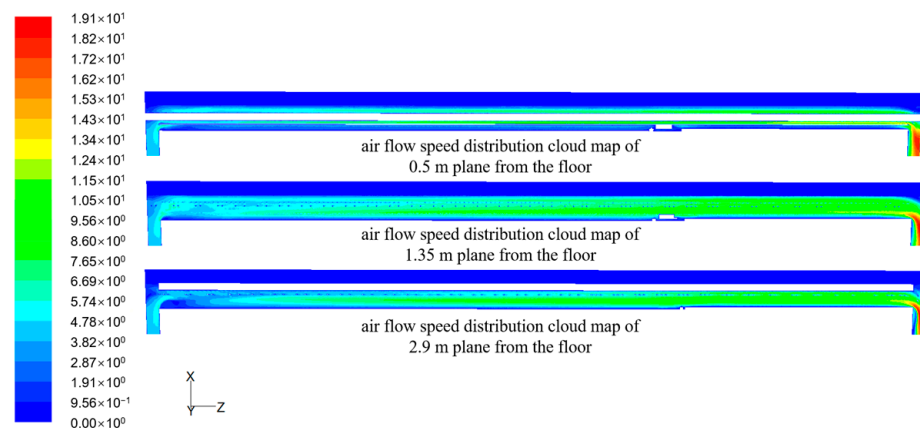


**Figure 3.** Airflow speed flow field distribution cloud of working face.

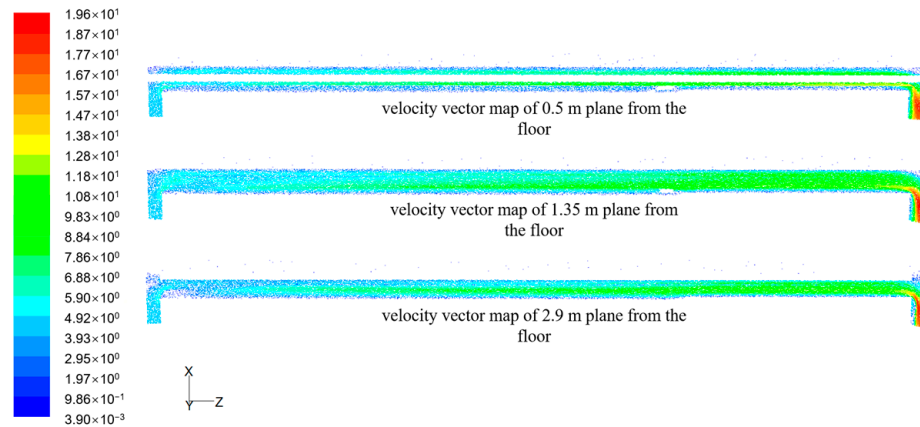


**Figure 4.** Airflow speed distribution vector map of working face.

It can be seen from the figure that the airflow speed distribution of the flow field in the working face is extremely uneven. Due to the large channel space and small resistance, the wind flow is mainly dominated by the channel space flow, which is hindered by the hydraulic prop. The airflow speed between the hydraulic prop and the coal chute is small. Due to the flow around the hydraulic prop, the flow field stability is poor, and it is easy to produce gas accumulation. During the working process of the shearer, it is easy to form a flow around it, and the flow field has a large disturbance phenomenon, forming a large range of eddy current area; in the process of transporting coal by the front and rear chutes, because the direction of movement is opposite to the direction of airflow flow, the flow field also has a certain disturbance effect, which affects the distribution of airflow.

*4.2. Simulation Study on Gas Concentration Distribution Law of Fully Mechanized Caving Face*

The working face adopts the U-shaped ventilation mode, the average airflow speed of the working face is set to 3.0 m/s, the advancing speed of the working face is 4.8 m/d, the desorption amount of coal seam gas is 3.9 m<sup>3</sup>/t, the desorption amount of coal body is 36 m<sup>3</sup>/min, the amount of gas in the goaf into the working face is 3.6 m<sup>3</sup>/min (10% of the amount of gas emission from the falling coal), and the amount of gas emission from the surrounding rock is 7.2 m<sup>3</sup>/min (20% of the amount of gas emission from the falling coal). The distribution of gas concentration along the 0.5 m, 1.35 m, and 2.9 m planes from the coal seam floor is shown in Figure 5, and the curve is shown in Figure 6.

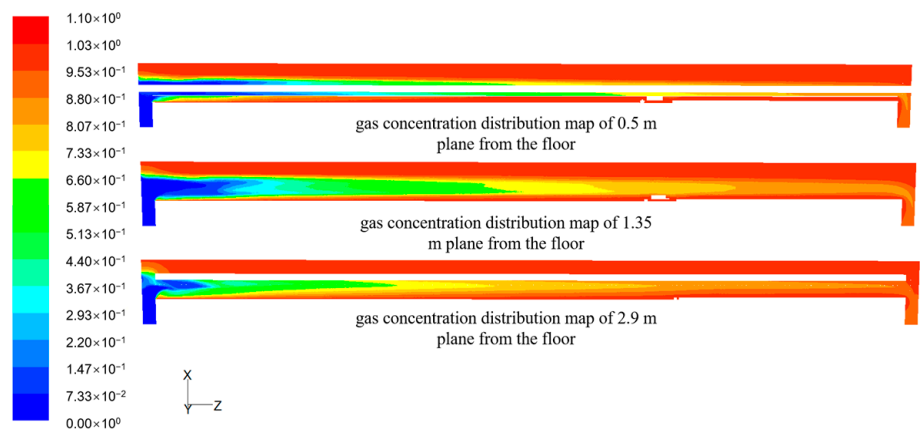


**Figure 5.** Gas concentration distribution cloud of working face.

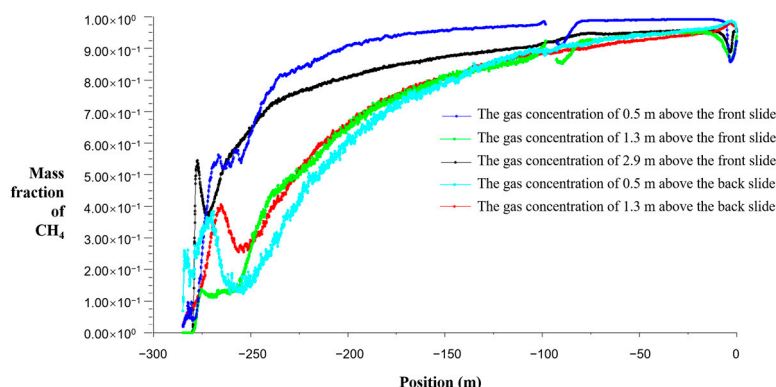


Figure 6. Gas concentration distribution curve of working face.

From the figure, it can be seen that the gas concentration of the working face gradually increases from the beginning of the air intake roadway, and the gas concentration reaches the maximum at the return air roadway. In the working face, the gas concentration is inversely proportional to the airflow velocity. In the same cross-section, the higher the airflow speed is, the lower the gas concentration is. The reason is that the existence of the airflow takes the gas away from the area, while the gas in other areas gradually enters the area in a diffusive way. The gas concentration between the hydraulic support and the ore-drawing chute is high and fluctuates greatly. The reason is that due to the existence of the hydraulic support, there is a phenomenon of flow around it, which leads to the fluctuation of gas concentration. There is a peak value of gas concentration fluctuation on the downwind side of the shearer at 3 m (equivalent to 8 m downwind of the rear drum), and the maximum peak value of gas concentration appears at the upper corner of the working face. This is mainly due to the high initial velocity of gas emission from the raw coal cut by the coal cutter. At the same time, it is affected by the shearer, and the airflow is disturbed, which affects the gas migration.

#### 4.3. Simulation Study on Gas Concentration Distribution Law of Working Face, Goaf and Upper Corner Under Different Airflow Speed Conditions

##### 4.3.1. Simulation Study on Gas Concentration Distribution Law of Working Face

In the case of other conditions unchanged, by changing the velocity inlet conditions, the average airflow speed of the working face is 1.5 m/s, 2.0 m/s, 2.5 m/s, 3.0 m/s, and 3.5 m/s, respectively. The gas concentration distribution along the 1.5 m plane from the coal seam floor is shown in Figure 7, the gas concentration distribution at the 2.5 m distance from the center line of the return air roadway to the coal seam floor is shown in Figure 8, and the gas concentration distribution curve at the upper corner is shown in Figure 9.

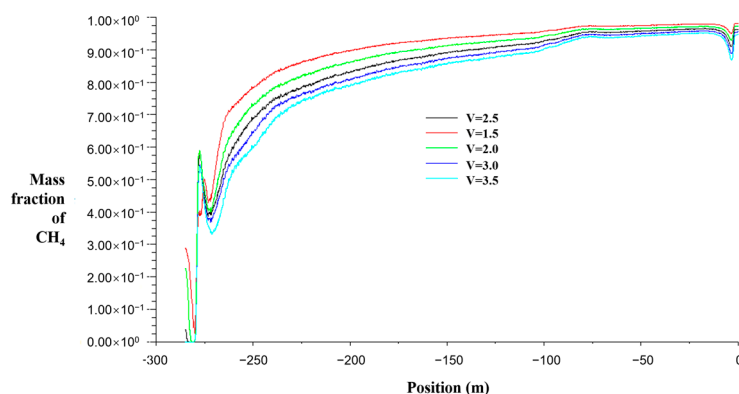
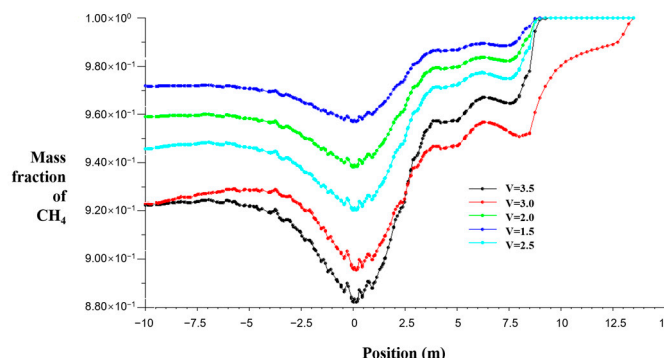
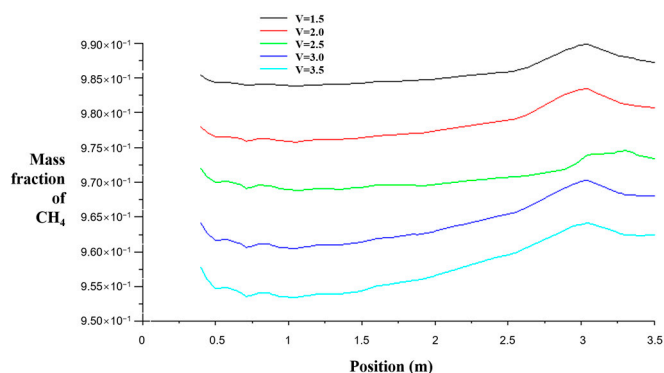


Figure 7. Gas concentration distribution curve of working face under different airflow speed conditions.



**Figure 8.** Gas concentration distribution curve of return airway center line under different airflow speed conditions.



**Figure 9.** Gas concentration distribution curve of upper corner under different airflow speed conditions.

It can be seen from the figure that the airflow speed of the working face directly affects the airflow of the working face. If the airflow speed is too low, the gas concentration will increase under the condition of the same gas release amount. The airflow speed also affects the stability of the airflow in the working face. The larger the airflow speed is, the worse the stability of the airflow is, and the wider the gas dissipation range in the working face is. The airflow velocity of the working face greatly influences the flow state of the airflow in the upper corner and the lower corner of the working face. When the airflow speed is too low, a large airflow vacuum zone will be formed at the upper corner. Due to the low airflow replacement rate, the gas concentration in this area will increase. When the airflow velocity is too large, it is easy to form a vortex zone at the upper corner. The gas-containing airflow stays too long at the upper corner, which also easily causes gas overruns.

#### 4.3.2. Simulation Study on Distribution Law of Gas Concentration in Goaf

From the floor  $z = 3$  m goaf gas concentration distribution cloud.

It can be seen from the Figure 10 that the gas concentration can be divided into three stages in the whole goaf trend: in the first 30 m near the working face, the gas concentration increases slowly, and the gas concentration is low; in the range of 30 m~160 m, the gas concentration increases rapidly, and there is obvious stratification. After 160 m, the growth of gas concentration gradually slowed down and eventually stabilized. Along the dip direction of the working face, the gas concentration distribution in the goaf shows a trend of increasing gas concentration from the intake side to the return side, especially the gas concentration on the return side of the working face.

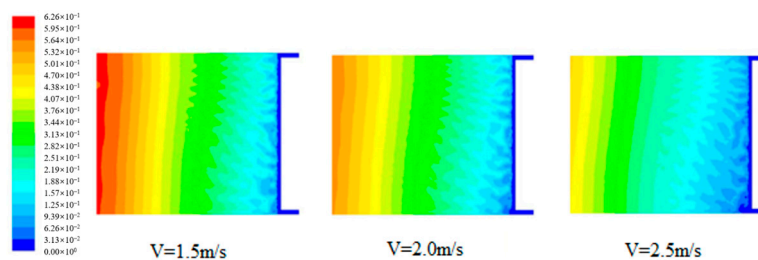


Figure 10. Under the U-shaped ventilation mode,  $v = 1.5 \text{ m/s}$ ,  $v = 2.0 \text{ m/s}$ ,  $v = 2.5 \text{ m/s}$ , the gas concentration cloud map is obtained.

#### 4.3.3. Simulation Study on Gas Concentration Distribution Law in Upper Corner

The change curve of gas concentration in the upper corner of the working face is shown in Figure 11.

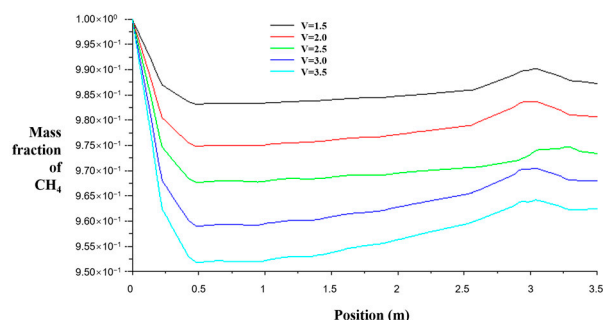


Figure 11. The change curve of gas concentration in upper corner under U-shaped ventilation mode.

It can be seen from Figure 11 that the change in airflow speed in the working face has a great influence on the gas concentration in the upper corner. However, in practical work, it should be determined by the amount of gas emission from the working face. For the fully mechanized caving face with large absolute gas emission, it is very limited to reduce the gas concentration in the upper corner and the return air side only by increasing the airflow speed (pressure difference). As the pressure difference increases, the air leakage volume will also increase, which will take away more gas from the goaf so that the gas concentration in the return air side and the upper corner will not decrease significantly or even increase.

#### 4.4. The Influence of Different Advancing Speed of Working Face on the Distribution Law of Gas Concentration in Upper Corner

In the simulation, the working face adopts U-type ventilation mode, the desorption capacity of coal seam gas is  $3.9 \text{ m}^3/\text{t}$ , the average airflow speed of the working face is  $3 \text{ m/s}$ , and the working face advancing speed is 4 (3.2 m), 5 (4.0 m), 6 (4.8 m), 7 (5.6 m), and 8 (6.4 m) cycles per day. The amount of desorption gas in mined-out coal is  $24 \text{ m}^3/\text{min}$ ,  $30 \text{ m}^3/\text{min}$ ,  $36 \text{ m}^3/\text{min}$ ,  $42 \text{ m}^3/\text{min}$ , and  $48 \text{ m}^3/\text{min}$ . The amount of gas emission in goaf is  $2.4 \text{ m}^3/\text{min}$ ,  $3.0 \text{ m}^3/\text{min}$ ,  $3.6 \text{ m}^3/\text{min}$ ,  $4.2 \text{ m}^3/\text{min}$ , and  $4.8 \text{ m}^3/\text{min}$ , respectively. The amount of gas emission in surrounding rock is  $4.8 \text{ m}^3/\text{min}$ ,  $6.0 \text{ m}^3/\text{min}$ ,  $7.2 \text{ m}^3/\text{min}$ ,  $8.4 \text{ m}^3/\text{min}$ , and  $9.6 \text{ m}^3/\text{min}$ , respectively. The change curve of gas concentration in the upper corner is shown in Figure 12.

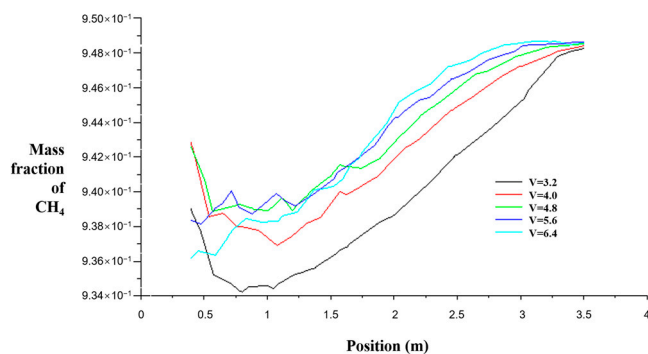


Figure 12. Gas concentration distribution curve of upper corner under different advance speed conditions.

It can be seen from the figure that when the advancing speed of the working face is four working face cycles, the gas concentration in the upper corner is the lowest, and the change is stable. With the increase in the advancing speed, the gas concentration gradually increases. When the advancing speed of the working face reaches eight working face cycles, the gas concentration in the upper corner is the highest, and the change is extremely unstable. This is mainly because the advancing speed of the working face is accelerated, the number of coal cuts per unit of time is increased, and the amount of gas released is increased, resulting in an increase in the gas concentration in the upper corner and obvious fluctuations. Therefore, it is more conducive to the discharge of gas in the upper corner by controlling the advancing speed of the working face in 5–7 working face cycles.

4.5. The Influence of Different Amount of Residual Coal in Goaf on the Distribution Law of Gas Concentration in Upper Corner of Working Face

In the simulation, the working face adopts a U-shaped ventilation mode, the residual gas volume of coal seam is  $3.9 \text{ m}^3/\text{t}$ , the advancing speed of the working face is  $4.8 \text{ m/d}$ , the recovery rate of the coal seam is 85%, 87.5%, 90%, 92.5%, and 95%, respectively, the gas emission volume of caving coal is  $36 \text{ m}^3/\text{min}$ , the gas emission volume of surrounding rock is  $7.2 \text{ m}^3/\text{min}$ , and the gas emission volume of goaf is  $10.8 \text{ m}^3/\text{min}$ ,  $9 \text{ m}^3/\text{min}$ ,  $7.2 \text{ m}^3/\text{min}$ ,  $5.4 \text{ m}^3/\text{min}$ , and  $3.6 \text{ m}^3/\text{min}$ . The distribution of gas concentration along the center line of the return airway is shown in Figure 13, and the change curve of gas concentration in the upper corner is shown in Figure 14.

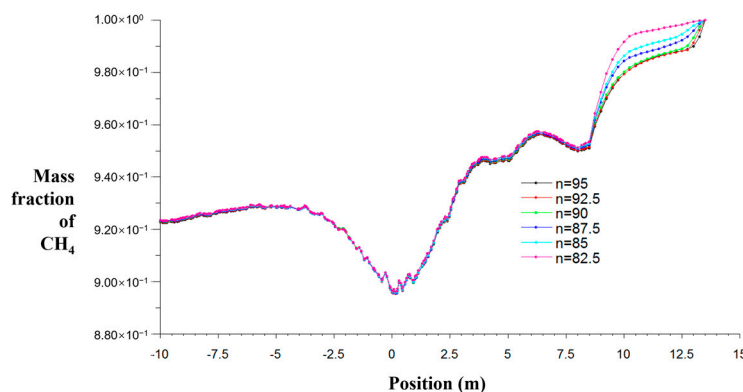


Figure 13. Gas concentration distribution curve of return airway center line under different recovery conditions.

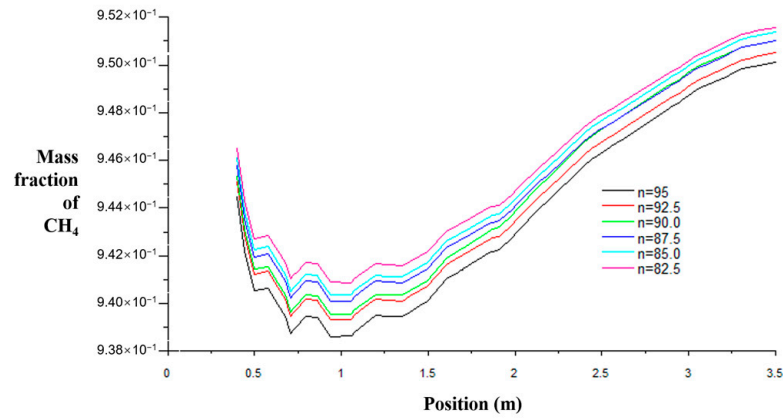


Figure 14. Gas concentration distribution curve of upper corner under different recovery conditions.

From the figure, it can be seen that the higher the recovery rate, the smaller the gas concentration in the upper corner, mainly because the higher the recovery rate, the less the amount of residual coal in the goaf, the less the amount of desorbed gas, and the less the amount of gas seeping into the goaf, resulting in a weak change in the gas concentration in the upper corner.

4.6. Simulation Study on Gas Migration Law in Goaf Under Different Ventilation Modes

4.6.1. Numerical Simulation of Gas Concentration Distribution Law in Goaf of Working Face Under U-Type Ventilation Mode

In the N2015 fully mechanized caving face, the actual air supply volume is 3000 m<sup>3</sup>/min. In the initial stage of mining, the air inlet roadway is set as the velocity inlet, the converted airflow speed is 2.85 m/s, the return air roadway is set as the free outlet, and the interface between the working face and the goaf is set as the porous jump condition. The desorption gas of the coal seam in the working face is 3.99 m<sup>3</sup>/t, and the absolute gas emission is 42.9 m<sup>3</sup>/min according to the recovery amount of 12,000 t/d. The velocity cloud figure of the goaf is shown in Figure 15, the velocity vector figure is shown in Figure 16, and the gas concentration distribution in the plane 1.5 m from the coal seam floor is shown in the figure.

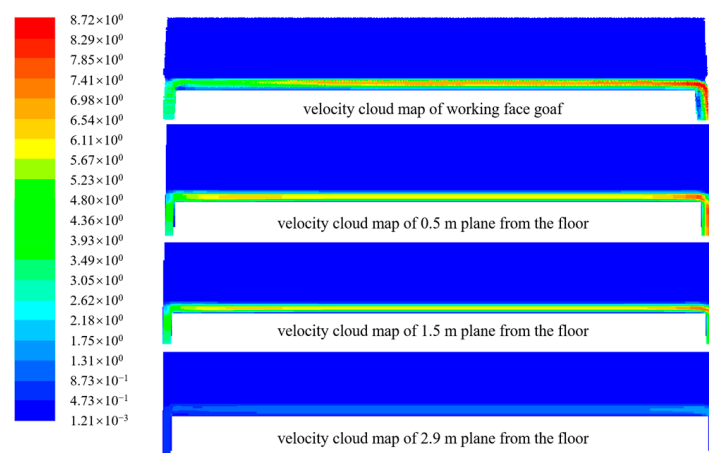


Figure 15. Speed cloud map before the first weighting of roof.

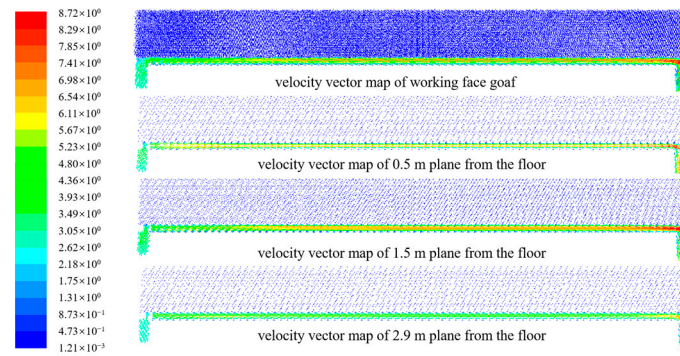


Figure 16. Velocity vector map before the first roof weighting.

From Figures 15 and 16, it can be seen that under the condition of U-shaped ventilation, the ventilation airflow mainly flows through the working face from the return air lane, and a very small part of the airflow bypasses the support between the working face and the goaf into the goaf. Affected by the support and the caving coal and rock mass, the airflow velocity entering the goaf decreases rapidly and tends to stop as the airflow speeds away from the working face. When the airflow moves in the working face, the airflow speed near the roof and floor is low, which is also one of the reasons for the high gas concentration near the roof of the working face.

#### 4.6.2. Numerical Simulation of Gas Migration Law in Goaf Under U + I and U + L Ventilation Modes

Based on the process parameters of the N2105 working face in the Yuwu Coal Industry, the working face is designed as U + I and U + L ventilation mode, and a three-dimensional geometric model of goaf in a fully mechanized caving face is established, which is 15 m in length, 5 m in width, and 3.5 m in height of intake and return air roadway; 15 m in length, 4.4 m in width, and 3 m in height of gas roadway; 10 m in the bottom surface of gas roadway from coal seam floor and 20 m in horizontal distance from return air roadway; 275 m in length, 5 m in width, and 3.5 m in height of working face; 285 m in length, 200 m in width, and 40 m in height of goaf, as shown in Figure 17.

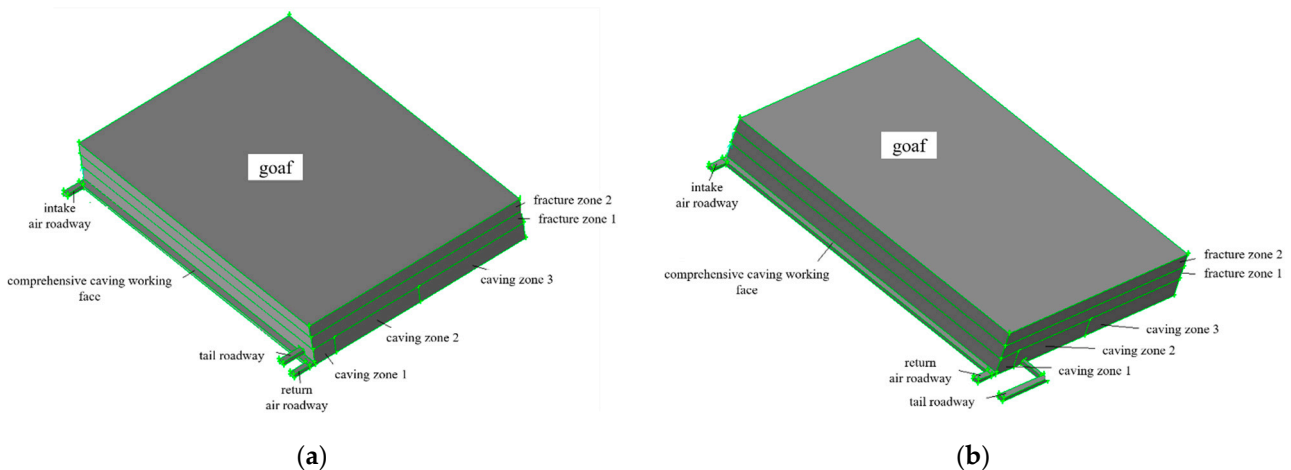
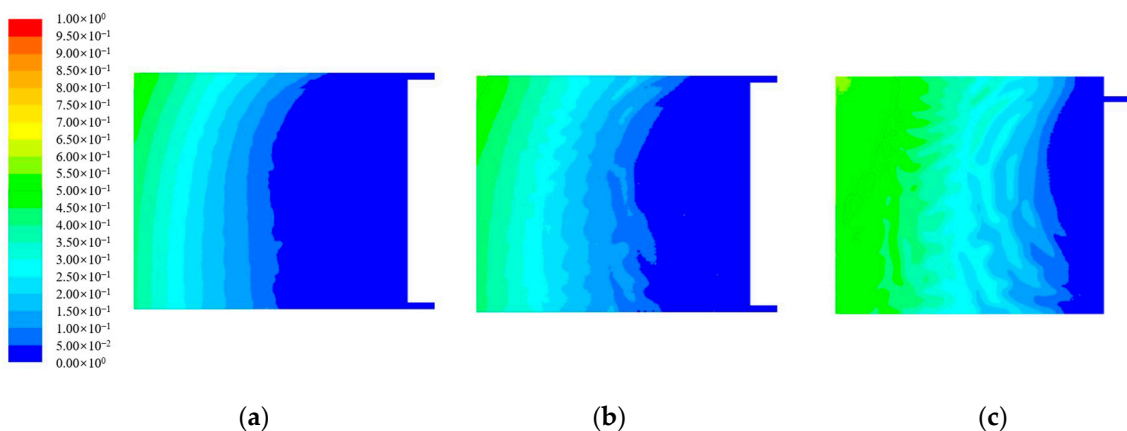


Figure 17. Geometric model of goaf under different types of ventilation modes: (a) the geometric model of goaf under U + I ventilation mode is established; (b) the geometric model of goaf under U + L ventilation mode is established.

Under the condition that other parameters remain unchanged, the inlet air lane is selected as the speed inlet, the airflow speed is 2.5 m/s, and the return air lane and the gas lane are free exits. The absolute gas emission in the goaf is 44.89 m<sup>3</sup>/min, respectively, to

simulate the distribution and migration law of gas concentration in the goaf when U + I and U + L ventilation modes are used.

Figures 18 and 19 are the gas concentration distribution cloud maps in the horizontal and vertical directions of the goaf under the U + I ventilation mode.



**Figure 18.** Gas concentration in different horizontal sections of goaf under U + I ventilation mode: (a) gas concentration in goaf at horizontal section position  $Z = 0$  m; (b) gas concentration in goaf at horizontal section position  $Z = 3$  m; (c) gas concentration in goaf at horizontal section position  $Z = 8$  m.

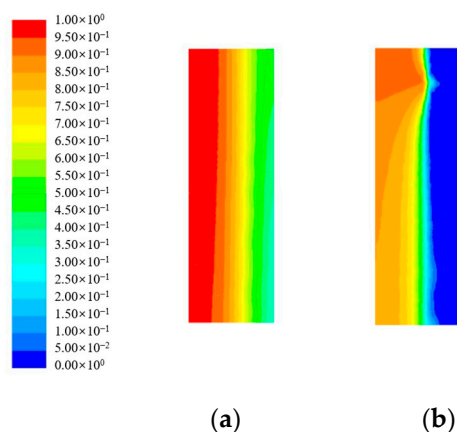


**Figure 19.** Gas concentration in different vertical sections of goaf under U + I ventilation mode: (a) gas concentration in goaf at vertical section  $x = 20$  m; (b) gas concentration in goaf at vertical section  $x = 265$  m.

It can be seen from the figure that compared with the U-type ventilation mode, some gas is discharged with the “I” lane in the U + I type, and the gas concentration in the upper corner and the support influence area can be effectively reduced in the horizontal direction. In the vertical direction, the stratification of gas concentration distribution in the deep goaf is more obvious. The reason for this phenomenon is that the gas in the shallow caving zone of the goaf is eliminated with the airflow of the gas roadway. The deep airflow speed in the goaf is very minimal, and the gas mainly depends on gravity and free diffusion. In addition, the viscous resistance coefficient of the fracture zone is large, the porosity is low, and the gas accumulation makes the concentration gradually increase.

Figure 20 shows that under the U + L ventilation mode, when the air volume ratio of the return air lane and the “L” lane is 2:1 (the airflow speed of the return air lane is 1.33 m/s, the airflow speed of the “L” lane is 0.67 m/s), 3:1 (the airflow speed of the return air lane is 1.5 m/s, the airflow speed of the “L” lane is 0.5 m/s), and 4:1 (the airflow speed of the return air lane is 1.6 m/s, and the airflow speed of the “L” lane is 0.4 m/s), the gas concentration distribution cloud map of the goaf.

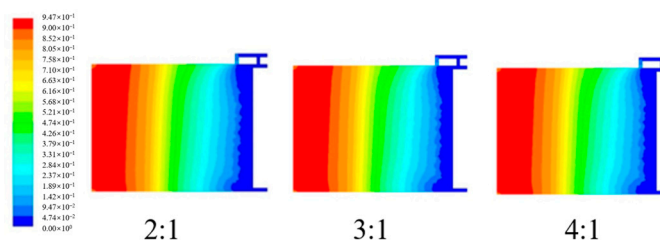


**Figure 20.** Gas concentration in goaf under U + L ventilation mode when air volume is 2:1, 3:1, 4:1.

It can be seen from the figure that due to the existence of the “L” roadway, the gas in the goaf flows to the “L” roadway with the airflow, so the concentration of the coal mining face and the return air roadway is low, and the gas concentration of the outer tail roadway is high. The influence of the tail roadway on the gas flow field in the goaf of the working face is mainly reflected near the upper corner. The farther away from the tail roadway, the smaller the change in gas concentration. The outer staggered tail roadway can effectively reduce the gas concentration in the upper corner and effectively alleviate the problem of gas overrun. By comparing the gas concentration distribution in the goaf with the air volume ratios of 2:1, 3:1, and 4:1 in the return air lane and the outer staggered tail lane, it can be seen that the concentration in the upper corner is significantly lower than that in the U-type ventilation. However, the change in air volume ratio has a limited impact on the gas concentration in the upper corner. If conditions permit, increasing the air volume of the outer staggered tail lane will help reduce the gas concentration in the gas tail lane and ensure safety.

## 5. Conclusions

In this study, the N2105 working face of Yuwu Coal Industry was taken as an example. By establishing the mathematical model of gas seepage in goaf and using ANSYS Fluent 6.3.26 for numerical simulation, the migration law of gas in goaf and its influencing factors were systematically analyzed. The research shows that the ventilation mode and the airflow speed of the working face have a significant influence on the distribution and change in gas concentration in the goaf, which provides a theoretical basis for reducing the risk of gas overrun in the working face.

If the airflow speed of the working face is too low, it is easy to cause gas accumulation. With the increase in the airflow speed of the working face, it is beneficial to discharge gas, but the increase in the airflow speed will also increase the gas seepage flow in the coal seam and goaf and increase the gas concentration in the working face and return airway. When the average airflow speed of the working face is about 3 m/s, the gas emission effect is the best under the condition of meeting other wind requirements such as dust emission.

Affected by the airflow speed of the working face, the air leakage in the goaf near the working face is large. With the increase in depth, the air leakage gradually decreases, and the gas accumulation is obvious. The goaf along the strike can be divided into three stages: in the first 30 m near the working face, the gas concentration increases slowly, and the gas concentration is low; in the range of 30~160 m, the gas concentration increases rapidly, and there is obvious stratification. After 160 m, the growth of gas concentration gradually slowed down and eventually stabilized, but the concentration can reach more than 90%.

Along the dip direction of the working face, the gas concentration distribution in the goaf shows a trend of increasing gas concentration from the inlet side to the return side, especially the gas concentration on the return side of the working face. The reason for this phenomenon is that in the early stage of coal release, the direct roof and the main roof are prone to the phenomenon of cantilever beam under the action of their own strength, and the caving rock in the goaf is freely accumulated, the porosity is large, and the air leakage

airflow speed is large. Part of the gas is easy to accumulate on the return air side and the upper corner.

The recovery rate of coal seam is directly reflected in the amount of residual coal in goaf. When the amount of residual coal is less, U-type ventilation mode should be selected. When there is more residual coal in goaf or more gas emission in adjacent layers, the U + I-type ventilation mode is easy to use. When the working face needs more air volume and more gas emission, U + L-type ventilation mode is easy to be used.

The influence of advancing speed of working face on gas concentration of working face is mainly reflected in the gas release intensity of mining coal. The faster the advancing speed of the working face, the more the mining coal, the greater the amount of gas released, and the higher the gas concentration of the working face. When the advancing speed of the working face is 5~7 working cycles, the gas concentration control effect of the working face is the best.

U-shaped ventilation has the smallest influence range on gas concentration in goaf. Under this ventilation mode, the fluctuation of gas concentration in the goaf is small, and its variation range is mainly affected by the airflow speed of the working face. This method is more suitable for low gas mines with less gas emission and can solve gas problems by ventilation. U + I type ventilation mode, that is, a special gas discharge roadway is dug at the roof of the coal seam. The tail end of the roadway is in the upper part of the collapsed coal and rock accumulation body in the goaf. Because the collapse of the coal seam roof is affected by the time effect, and the gap between the coal and rock mass is large at the initial stage of collapse, it is more conducive to the migration of gas. Therefore, it is more effective for the gas control in the working face of high gas and thick coal seam mining. The U + L type ventilation mode is based on the U type ventilation mode, and a gas roadway parallel to the return air trough is arranged. The roadway spacing is 15–20 m. During the excavation process, a certain distance is connected at each interval to form a contact roadway. Because the gas roadway is not destroyed during the mining process, it is beneficial for the high-concentration gas in the goaf to flow into it and effectively reduce the gas concentration flowing into the working face from the upper corner. The ventilation method solves the problem of high gas concentration in the upper corner of the working face due to the influence of air volume.

**Author Contributions:** Formal analysis, writing—original draft preparation, investigation, H.W. and R.G.; supervision, conceptualization, methodology, resources, validation, H.A. and X.L. All authors have read and agreed to the published version of the manuscript.

**Funding:** This research was supported in part by the Yunnan Fundamental Research Projects (NO. 202401CF070138), and Yunnan Province “Caiyun” Postdoctoral Innovative Project Plan (No. CG24056E004A).

**Institutional Review Board Statement:** Not applicable.

**Informed Consent Statement:** Not applicable.

**Data Availability Statement:** Data are available from the corresponding author upon request.

**Conflicts of Interest:** The authors declare no conflicts of interest.

## References

1. Zhang, W.; Zhao, B.; Guo, X.; Deng, C.; Gao, J. Gas migration law of gas-bearing rock strata under the influence of repeated mining. *Min. Saf. Environ. Prot.* **2024**, *51*, 61–69. [[CrossRef](#)]
2. Zhang, D.M. Research on Numerical Simulation Method of CBM Directional Horizontal Well Mining. Ph.D. Thesis, Graduate School of Chinese Academy of Sciences, Beijing, China, 2004.

3. Ding, H.C. Study on Gas Migration Law and Drainage Technology in Goaf of Fully Mechanized Mining Face in Zhangji Coal Mine Beijing. Ph.D. Thesis, University of Science and Technology Beijing, Beijing, China, 2008.
4. Tang, Y. Research on gas prevention and control technology in fully mechanized mining face of single permeability outburst thick coal seam. *Inn. Mong. Coal Econ.* **2018**, *123–124*. [[CrossRef](#)]
5. Aguado, M.B.D.; Nicieza, C.G. Control and prevention of gas outbursts in coal mines, Riosa–Olloniego coalfield, Spain. *Int. J. Coal Geol.* **2007**, *69*, 253–266. [[CrossRef](#)]
6. Zhu, Z.; Guo, L.; Wang, X. Optimization of ventilation system in Liuzhuang coal mine. *Coal Mine Saf.* **2011**, *42*, 103–106.
7. Zhao, J.Q. Analysis of Influence Factors and Rules of Gas Emission in Fully mechanized top coal caving face. *Coal Mine Mod.* **2013**, 48–50. [[CrossRef](#)]
8. Hao, Y.; Wang, F.; Wang, X.; Liu, X. Research of gas movement law in goaf with parallel double U-shape ventilation mode. *J. Mine Autom.* **2014**, *40*, 41–44. [[CrossRef](#)]
9. Karacan, C.Z. Analysis of gob gas venthole production performances for strata gas control in longwall mining. *Int. J. Rock Mech. Min. Sci.* **2015**, *79*, 9–18. [[CrossRef](#)]
10. Li, Y.Q. Gas Control Mode of Outburst Coal Seams in Huainan Coal Mining Area. *Coal Technol.* **2016**, *35*, 222–223. [[CrossRef](#)]
11. Zhang, X.C. Research on comprehensive gas extraction technology in high-gassy coal seam group. *China Coal.* **2018**, *44*, 108–112. [[CrossRef](#)]
12. Chang, W. Exploration and Practice of Gas Control Technology in Fully Mechanized Caving Face. *Tongmei Sci. Technol.* **2022**, 41–45. [[CrossRef](#)]
13. Zhou, Y.; Hu, Y.Y.; Tao, M.D. Research and application of high level drainage roadway in fully mechanized mining face. *Shandong Coal Sci. Technol.* **2022**, *40*, 127–129.
14. Shi, L.L. Research and application of gas control technology in goaf of fully mechanized mining face. *Shanxi Metall.* **2022**, *45*, 309–311. [[CrossRef](#)]
15. Huang, M.Z. Theory of Gas Occurrence and Flow in Coal Seam. *Energy Energy Conserv.* **2016**, 8–9+85. [[CrossRef](#)]
16. Lin, F.H.; Wei, W.B.; Li, S.G. Experiment study on effects of factors on gas adsorption of coal sample. *China Saf. Sci. J.* **2015**, *25*, 121–126. [[CrossRef](#)]
17. Xin, Y.L. Gas Extraction Technology of Slicing in High Gas Thick Seam. *Mech. Manag. Dev.* **2017**, *32*, 165–167. [[CrossRef](#)]
18. Zhou, T.Y.; Li, Q.F. Study on gas control technology in slicing mining of high gas thick coal seam. *Coal Eng.* **2017**, *49*, 53–57+61.
19. Karacan, C.Ö. Predicting methane emissions and developing reduction strategies for a Central Appalachian Basin, USA, longwall mine through analysis and modeling of geology and degasification system performance. *Int. J. Coal Geol.* **2023**, *270*, 104234. [[CrossRef](#)]
20. Soleimani, F.; Si, G.Y.; Roshan, H. Numerical modelling of coal and gas outburst initiation using energy balance principles. *Fuel J. Fuel Sci.* **2023**, 334. [[CrossRef](#)]
21. Szott, W.; Słota-Valim, M.; Gołabek, A.; Sowizdżał, K.; Łętkowski, P. Numerical studies of improved methane drainage technologies by stimulating coal seams in multi-seam mining layouts. *Int. J. Rock Mech. Min. Sci.* **2018**, *108*, 157–168. [[CrossRef](#)]
22. Hu, Q.-T.; Liang, Y.-P.; Liu, J.-Z. CFD simulation of goaf gas flow patterns. *J. China Coal Soc.* **2007**, *32*, 719–723.
23. Li, Z.X. Study on numerical simulation of gas eission regularity and boundary condition of the goaf in coal caving of the fully-mechanized. *Journal of China Coal Society.* **2002**, *27*, 173–178.
24. Zhang, Y.Z. Experimental Study on Gas Concentration Distribution and Migration law in Goaf of Fully Mechanized Mining Face. Master’s Thesis, Taiyuan University of Technology, Taiyuan, China, 2011.
25. Yu, Y.-N.; Qin, R.X.; Cui, Y. Numerical Simulation of Gas Field and Air Leakage Field in Gob with Y-type Ventilation. *Safety in Coal Mines.* **2013**, *44*, 25–28. [[CrossRef](#)]
26. Wu, S.Y.; Guo, Y. Gas control of mechanical mining coal face of high yield using Y model ventilation manner. *J. Xi’an Univ. Sci. Technol.* **2001**, *21*, 205–207.
27. Zhang, H.S. Numerical Simulation of Flow Field and Gas Migration Law in Goaf. Master’s Thesis, Hebei University of Engineering, Handan, China, 2013.
28. Zheng, Q.Y. Numerical Simulation Accuracy and Parallel Computing of Complex Flows Based on Navier-Stokes Equations. Ph.D. Thesis, Xi’an University of Electronic Science and Technology, Xi’an, China, 2011.
29. Duan, S.; Nie, B. Preliminary study on diffusion-seepage law of coal seam gas. *J. Taiyuan Univ. Technol.* **1998**, *29*, 413–417.
30. Zhang, D.M.; Liu, J.Z. Regularity on the distribution of gas moving in gob area of coal mine. *Chin. J. Geol. Hazard Control.* **2003**, *14*, 81–84.
31. Tan, X.; Yuan, J. Study on the real gas seepage equation of mine coal seam. *J. Chongqing Univ. Civ. Eng.* **1986**, 106–112.
32. Wu, Y.G.; Wu, J.M.; Wang, J.F.; Zhou, C.S. The law of gas distribution in goaf of fully mechanized top-coal caving working face with “double-U” ventilation system. *J. China Coal Soc.* **2011**, *36*, 1704–1708.
33. Ding, H. Numerical simulation and experiment research on gas migration in goaf under U + L type ventilation. *J. Nat. Disasters* **2012**, *21*, 192–198.

34. Lan, Z.Q.; Zhang, G.S. Numerical simulation of gas concentration field in multi-source and multi-congruence goaf. *J. China Coal Soc.* **2007**, *32*, 396–401.
35. Liang, Y.; Hu, Q.; Zhang, J. Study on the law of gas flow in the goaf of Xieqiao Mine. *Min. Saf. Environ. Prot.* **2006**, *33*, 1–6.
36. Li, C.G.; Wang, S.L.; Zheng, H.; Ge, X.R. Relationship between bulk modulus and porosity of porous medium. *Yantu Lixue (Rock Soil Mech.)* **2007**, *28*, 293–296.
37. Long, Q.M.; Zhao, X.S.; Sun, D.L.; Zou, Y.H. Experimental study on coal permeability by adsorption. *Meitan Xuebao/J. China Coal Soc.* **2008**, *33*, 1030–1034.
38. Gao, J.; Li, X.X.; Cui, Y.K. Numerical simulation for airflow and gas distribution regulation in the goaf of mechanized working face. *J. Saf. Environ.* **2013**, *13*, 164–168.
39. Sun, Y.; Yang, S.Q.; Ling, Z.Q. Analysis of gas migration law in goaf of fully mechanized caving face with large mining length. *Coal Mine Saf.* **2009**, *40*, 13–16.
40. Zhang, Y.S. Gas control technology in fully mechanized mining face. *Ind. Technol.* **2013**, 81–82.

**Disclaimer/Publisher’s Note:** The statements, opinions and data contained in all publications are solely those of the individual author(s) and contributor(s) and not of MDPI and/or the editor(s). MDPI and/or the editor(s) disclaim responsibility for any injury to people or property resulting from any ideas, methods, instructions or products referred to in the content.